Computers & Fluids xxx (2011) xxx–xxx

Contents lists available at SciVerse ScienceDirect

Computers & Fluids

journal homepage: www.elsevier.com/locate/compfluid

Cross wind effects on a simplified car model by a DES approach

Emmanuel Guilmineau *, Oussama Chikhaoui, GanBo Deng, Michel Visonneau

Equipe Modélisation Numérique, Laboratoire de Mécanique des Fluides, CNRS UMR 6598, Ecole Centrale de Nantes, BP 92101, 44321 Nantes Cedex 3, France

ARTICLE INFO

Article history:
Received 15 November 2010
Received in revised form 20 June 2011
Accepted 30 August 2011
Available online xxxx

Keywords:
Cross wind effects
Generic car model
DES
Vehicle aerodynamics

ABSTRACT

The paper presents a finite-volume-based Detached-Eddy Simulation for the prediction of flow around a passenger vehicle. The flow solver used is ISIS–CFD, developed by the CFD Department of the Fluid Mechanics Laboratory of Ecole Centrale de Nantes. This article presents a cross wind simulation around the square-back Willy model for several yaw angles. The model was designed in order that separations are limited to the region of the base for moderate yaw angles. This model without sharp corners on the fore body and a square base is designed to facilitate the analysis of separations which are, in that case, limited to its leeward side and base. The angle between the upstream velocity and the direction of the model varies from 0° and 30°. The results are compared to a previous numerical study based on a RANS simulation and experimental data at the Reynolds number $Re = 0.9 \times 10^6$. All comparisons (aerodynamic forces, wall pressures, and total pressure) show that DES simulations provide a better agreement with experimental data than isotropic or anisotropic statistical models, particularly for large yaw angles.

1. Introduction

In the development process of a new road vehicle, aerodynamic performance is mostly evaluated through the time-averaged forces and moments acting on the body. Such evaluation can be performed either by conventional wind tunnel measurements or by Computational Fluid Dynamics (CFD) based on the resolution of Reynolds Averaged Navier–Stokes (RANS) equations, assuming that the incoming flow is uniform with turbulence. On the other hand, increasing attention is paid to the unsteadiness of aerodynamics under real driving conditions such as strong gusty cross wind, sudden steering, passing or crossing maneuvers as well. In fact, transient aerodynamics is mandatory to achieve higher vehicle driveability or increase the safety [12]. Indeed, the yawing moment, which is due to the side-force distribution, as well as the global side force are responsible for vehicle stability under cross winds. The existence of this moment causes a car to turn out of the wind, away from its driving direction.

Numerical simulation is well integrated in the automotive industry and is now an engineering tool used in parallel with experiments performed during the design process of road vehicles. Much fundamental research is performed on the Ahmed body, which includes most of the aerodynamic features found on a real car. This simplified vehicle geometry has been widely used in several experiments [1,20], and many numerical simulations have been performed to evaluate CFD tools and their ability to predict drag and lift for several slant angles [9,2,15,31,17,5,26]. In all these numerical studies, several methods were used to model turbulence: classic statistical turbulence models such as $k-\varepsilon$, the Detached Eddy Simulation (DES) or Large Eddy Simulation (LES). The LES results [17] were found to provide the best agreement with the experimental data [20], although these computations were conducted at a Reynolds number lower than the experiments. In experiments, the Reynolds number, based on the height of the model and the upstream velocity, is 7.68×10^5 while in their simulation, Krajnović and Davidson [17] used 2.8×10^5. They did not use the correct Reynolds number because the spatial resolution in the y direction on the top and the roof and in the z direction on the lateral sides could not be obtained for the experimental Reynolds number with the computational resources available at that time. Other attempt to simulate the Ahmed body flow by using LES was reported by Minguez et al. [26]. A LES with high order discretization scheme based on spectral approximations stabilized by spectral vanishing viscosity was employed. They successfully simulated the flow topology for the critical case with 25° slant angle, namely a partial separation of the turbulent boundary layer at the edge of the slant as observed in the measurement. However, a separation of the flow at front body was also predicted, resulting in wrong velocity profiles just before the beginning of the slant. Although this kind of front body separation has been observed in experiments performed at a much lower Reynolds number ($Re = 8322$) [34], it is not clear whether this separation is present in experiments at the Reynolds number they investigated. Hence, the successfulness in the prediction of flow topology of their simulation was not fully convincing.

While LES method requires large computing resources for high Reynolds number flows, Spalart et al. [33] proposed a hybrid

* Corresponding author. Tel.: +33 2 40 37 16 81; fax: +33 2 40 37 25 23.
E-mail address: Emmanuel.Guilmineau@ec-nantes.fr (E. Guilmineau).

0045-7930/$ - see front matter © 2011 Elsevier Ltd. All rights reserved.
doi:10.1016/j.compfluid.2011.08.020

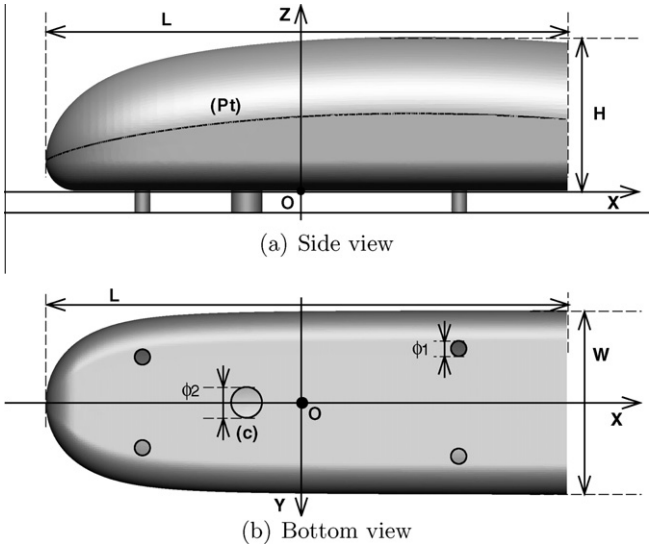

Fig. 1. Model definition.

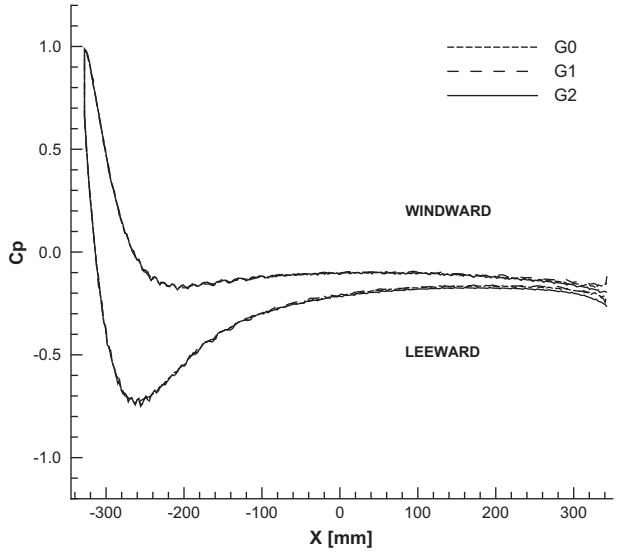

Fig. 2. $\beta = 10°$: Pressure coefficient along curve (Pt) versus the mesh.

approach, called Detached Eddy Simulation (DES), which combines features of Reynolds Averaged Navier–Stokes (RANS) formulations with LES methods. In the intial version, the RANS model was based on the Spalart–Allmaras model [32]. The concept is based on the idea of predicting the boundary layer by a RANS model and of switching the model to a LES model in detached regions. Later on, Strelets [35] proposed a DES-type hybrid method based on the Shear-Stress Transport (SST) model by introducing a length scale L_t in the turbulent kinetic energy transport equation. Menter and Kuntz [24] developed a delayed-DES method based on the SST model, which acts as the RANS model near the wall and prevents the pre-switching from RANS to LES due to the locally refined grids.

Historically, the cross wind effects on ground vehicle were first performed on trains [16,10] and shortly after on trucks [22,21,37] because of the size of the lateral side of these vehicles. On a modern heavy vehicle, one of the main sources of aerodynamic drag is the tractor–trailer gap drag, which occurs when the vehicle is operating in a cross wind [27]. Later the interest turned towards automobile because of a rising demand for safety and driving comfort. The most

Table 1
Characteristics of the meshes.

	G0	G1	G2
Number of points	1,609,155	6,651,159	10,808,408
Number of points on the model	30,905	102,522	205,366
Number of points on the ground	20,848	49,857	61,313
Number of cells	1,549,482	6,478,457	10,503,589

Table 2
$\beta = 10°$: Drag coefficient versus the mesh

	G0	G1	G2
Cx	0.3583	0.3665	0.3666

Table 3
Characteristic length scales evaluated for the Willy model body flow at Re = 900,000.

	l_0	l_{EI}	λ_T	l_{DI}	η	η_{mw}
Im (mm)	810	135	3.9	1.7	0.03	0.023
Dimensionless	1.2	2×10^{-1}	5.8×10^{-3}	2.5×10^{-3}	4.1×10^{-5}	3.4×10^{-5}

Table 4
Spatial resolution of the mesh.

	$y^+ = n\ u^*/\nu$	$s^+ = \Delta s\ u^*/\nu$	$l^+ = \Delta l\ u^*/\nu$
Mean	0.19	85.65	66.71
Maximum	0.65	170	180

conventional method to assess the stability in a cross wind condition is based on the quasi-steady method. Thus, the mean aerodynamic forces are measured in a wind tunnel at various yaw angles in a stationary state. However, this approach is applicable only when the wind gust produces a small relative yaw angle. For high relative yaw angles, transient effects became significant [3], invalidating the quasi-steady hypothesis. Some numerical simulations of transient flow around a vehicle with the dynamic yaw-angle change were also recently performed with a LES method but these simulations require very significant computational ressources [36].

This article is devoted to the study of the aerodynamic characteristics of a generic model in a steady cross wind. The technique used to simulate this condition is to yaw the model relatively to the freestream flow. The model used is the Willy model which is well suited to the analysis of separations limited to its leeward side and base, since there are no sharp corners on the fore body that may otherwise lead to fore body separation. The results presented deal with the analysis of mean flow for various yaw angles β from $\beta = 0°$ to $\beta = 30°$. The method used in this paper is a DES approach and these results are compared to a previous numerical study conducted with a statistical RANS simulation and experimental data [8].

2. Willy model

Numerical simulations are performed on the square-back Willy model which was designed to satisfy the following criteria:

1. The geometry is realistic, compared with a real vehicle.
2. The model's plane underbody surface is parallel to the ground.
3. The separations are limited to the region of the base for a moderate yaw angle, i.e. $\beta = 10°$.

Please cite this article in press as: Guilmineau E et al. Cross wind effects on a simplified car model by a DES approach. Comput Fluids (2011), doi:10.1016/j.compfluid.2011.08.020

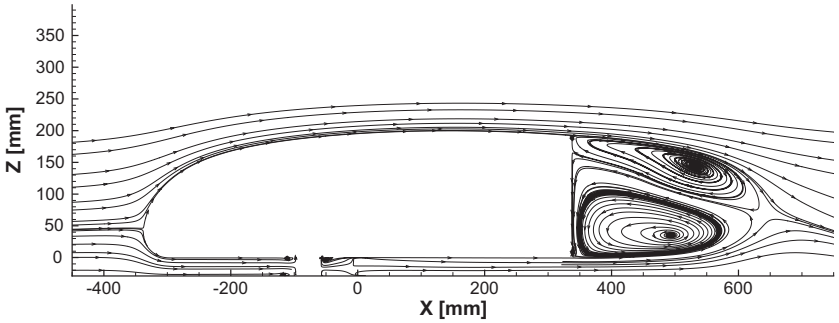

Fig. 3. $\beta = 0°$: Streamlines in the symmetry plane.

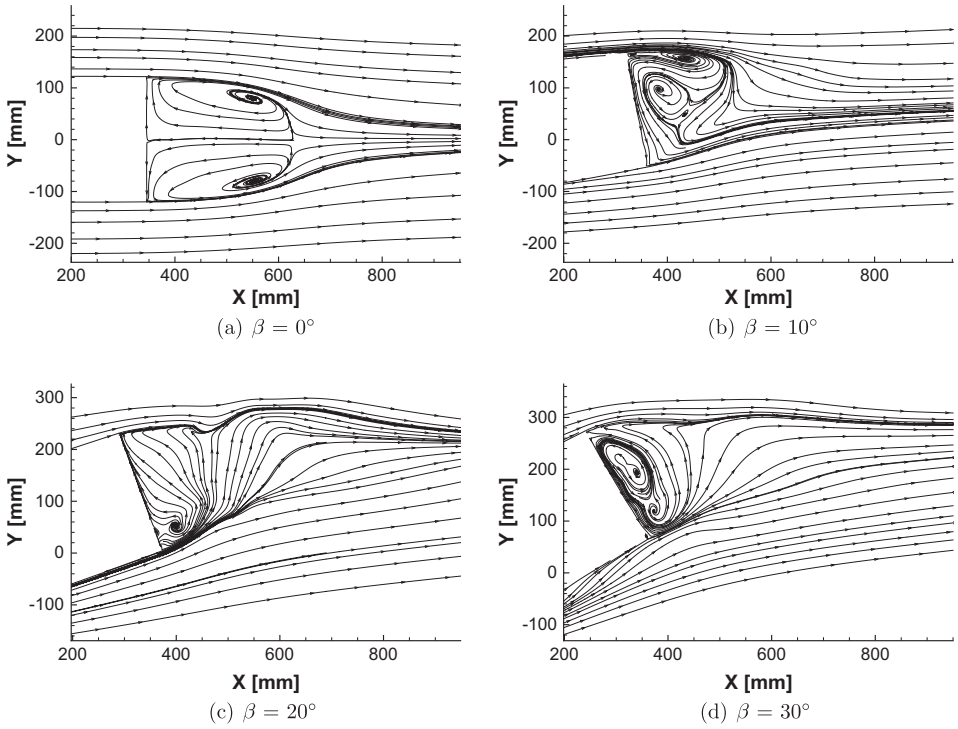

Fig. 4. Time-averaged streamlines at $Z/L = 0.1588$.

This model was first investigated by Chometon et al. [4]. The global view of the model is presented in Fig. 1.

The length of the model is $L = 675$ mm, the width is $W = 240$ mm, the maximum height is $H = 192$ mm and its surface reference is the maximum cross section $S_{ref} = 41{,}791$ mm^2. The ground clearance is $G = 29$ mm, and the diameter of the four feet (f), which are used to secure the model to the floor of the wind tunnel, is $\phi 1 = 20$ mm. A cylinder (c) with a diameter $\phi 2 = 40$ mm is used in experiments to protect the pressure tubes passing from the pressure taps to the multimanometer. Other dimensions are defined in [8]. The (P_t) line indicated in the figure is the position, where the measurements of pressure will be used for comparison later in this paper.

Two coordinate systems are distinguished. One is wind-tunnel fixed (Xo, Yo, Zo), Xo being parallel to the upstream velocity V_0. The other one is model fixed (X, Y, Z). The origin of the axes lies at point O located on the floor of the model and at 330 mm of the front of the model, see Fig. 1. This point O is the center of rotation of the model.

Cross flow is simulated by turning the Willy model with respect to the upstream velocity by an angle β, called yaw angle. The value of this angle is positive when the right side of the car model is windward. Experiments have been undertaken in the CNAM wind tunnel which has a cross section of 1.45×1.45 m^2 and a fixed ground. Air velocity, U_∞, in the wind tunnel has been fixed to 20 m/s, corresponding to a Reynolds number $\mathrm{Re} = 0.9 \times 10^6$, based on the length of the model L. As the Reynolds number is not too high, LES computations were performed on the same geometry and with the same condition by Krajnović and Sarmast [18]. In these simulations, the fine mesh contains between 9.1 and 9.8 million nodes according to the yaw angle. The same geometry, but without the central cylinder, was also studied experimentally by Gohlke et al. [6] who used Laser Dopler Velocimetry (LDV) in addition to force and pressure measurements. However, the Reynolds number, based on the upstream velocity and the length of the model, was 2.2×10^6. These authors also studied numerically two yaw angles with the Lattice Boltzmann method [7].

3. Numerics

3.1. Flow solver

The ISIS–CFD flow solver, developed by the Equipe Modélisation Numérique (EMN) of the Fluid Mechanics Laboratory of Ecole Cent-

Please cite this article in press as: Guilmineau E et al. Cross wind effects on a simplified car model by a DES approach. Comput Fluids (2011), doi:10.1016/j.compfluid.2011.08.020

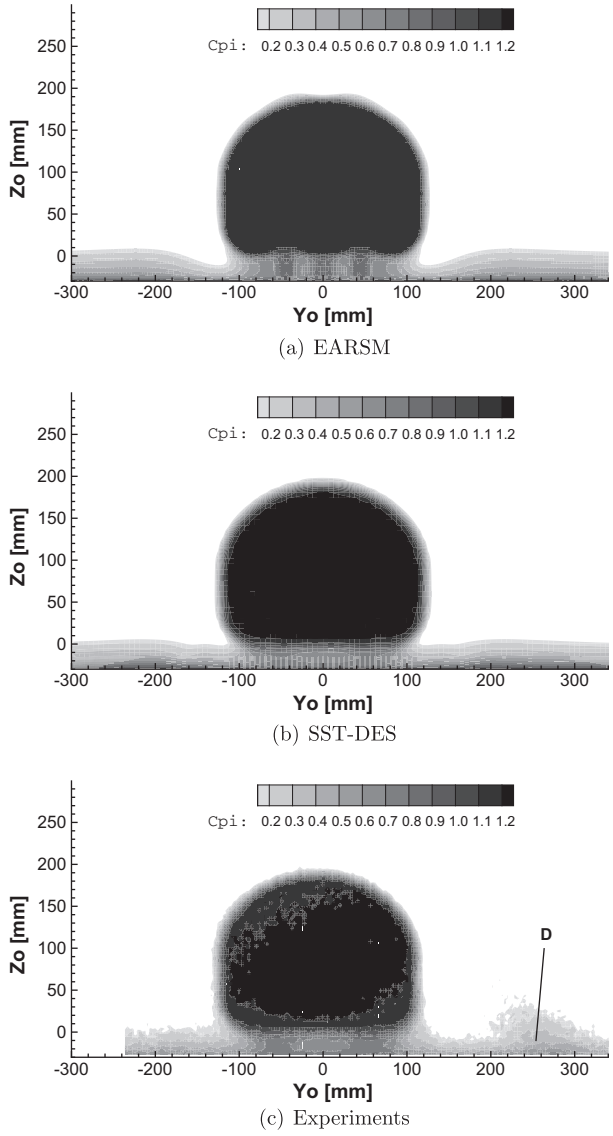

(a) EARSM

(b) SST-DES

(c) Experiments

Fig. 5. Total pressure coefficient for the yaw angle $\beta = 0°$ in the Xo-plane Xo/$L = 0.60$.

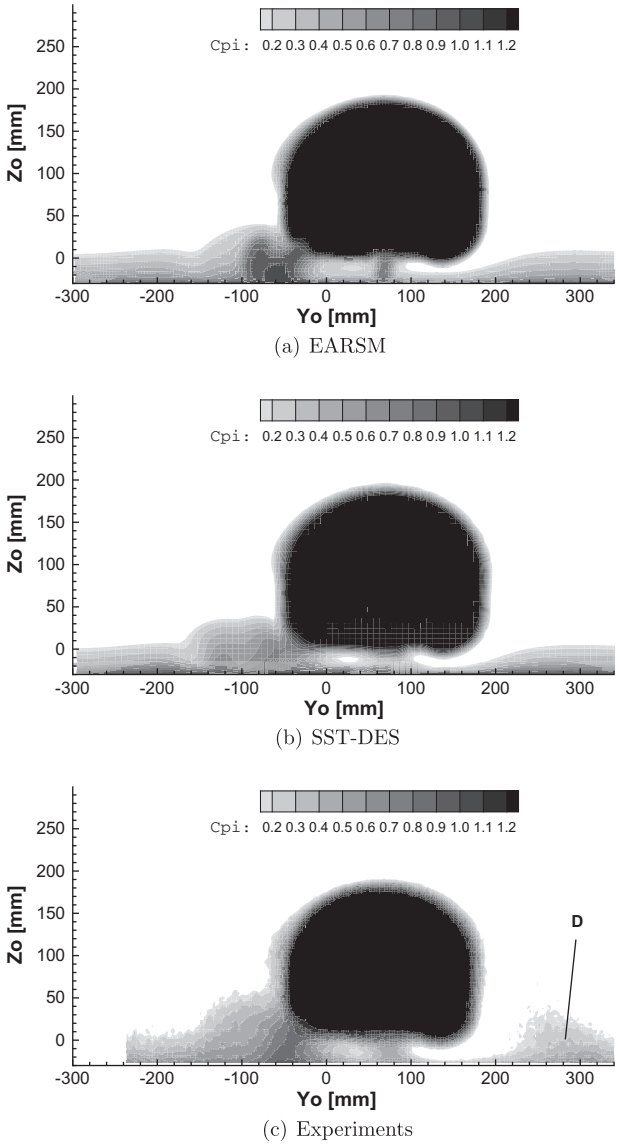

(a) EARSM

(b) SST-DES

(c) Experiments

Fig. 6. Total pressure coefficient for the yaw angle $\beta = 10°$ in the Xo-plane Xo/$L = 0.60$.

rale de Nantes [29], solves the incompressible unsteady Reynolds-Averaged Navier–Stokes equations. This solver is based on finite volume method to build a spatial discretization for the transport equations.

The incompressible unsteady Reynolds-Averaged Navier–Stokes equations can be written (using the generalized form of Gauss' theorem) as:

$$\frac{\partial}{\partial t}\int_V \rho\, dV + \int_S \rho(\vec{U} - \vec{U}_d)\cdot\vec{n}\, dS = 0 \tag{1a}$$

$$\frac{\partial}{\partial t}\int_V \rho U_i\, dV + \int_S \rho U_i(U_j - U_{dj})\cdot n_j\, dS = \int_S (\tau_{ij} n_j - p n_i) dS \tag{1b}$$

where V is the domain of interest, or control volume, bounded by a closed surface S moving at a velocity $\vec{U}_d$ with a unit outward normal vector $\vec{n}$, where n_j is the jth component. $\vec{U}$ and p are respectively the velocity and pressure fields. τ_{ij} are the components of the Reynolds stress tensor.

All flow variables are stored at the geometric center of arbitrary shaped cells. Volume and surface integrals are evaluated with second-order accurate approximations. The face-based method is generalized to two-dimensional or three-dimensional unstructured meshes for which non-overlapping control volumes are bounded by an arbitrary number of constitutive faces, that means cells can be polyhedra. A centered scheme is used for the diffusion terms, whereas for the convective fluxes, the Gamma Differencing Scheme (GDS) [14] is used for this study. Through a Normalized Variable Diagram (NVD) analysis [19], this scheme enforces local monotonicity and convection boundedness criterion. For more informations, see Queutey and Visonneau [29].

The velocity field is obtained from the momentum conservation equations, and the pressure field is extracted from the mass conservation constraint, or continuity equation, transformed into a pressure-equation. The pressure equation is obtained in the spirit of Rhie and Chow [30]. Momentum and pressure equations are solved in a segregated manner as in the SIMPLE coupling procedure [13].

A second-order backward difference scheme is used for time discretization. All spatial terms appearing in Eqs. (1a) and (1b) are treated in a fully implicit manner. In this paper, the geometry is fixed. Therefore, the velocity $\vec{U}_d$ in the Eqs. (1a) and (1b) is null.

Please cite this article in press as: Guilmineau E et al. Cross wind effects on a simplified car model by a DES approach. Comput Fluids (2011), doi:10.1016/j.compfluid.2011.08.020

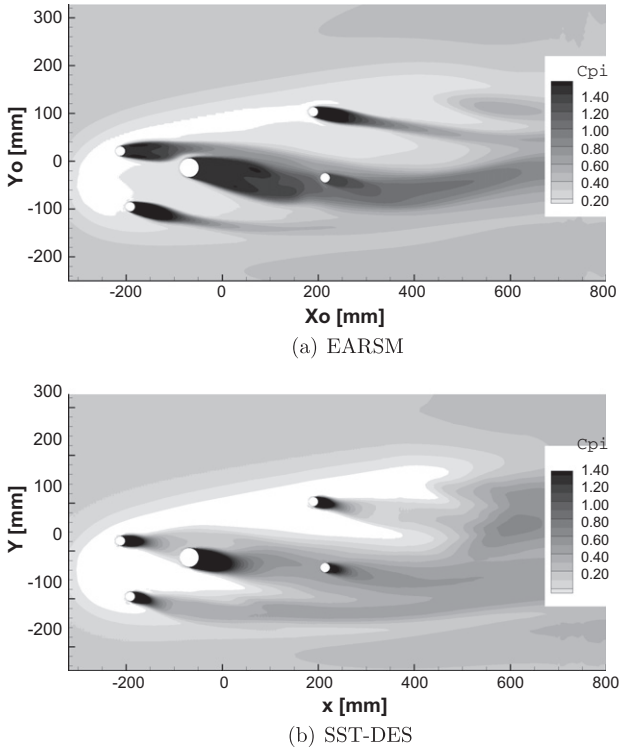

(a) EARSM

(b) SST-DES

Fig. 7. Total pressure coefficient for the yaw angle $\beta = 10°$ at Zo = −14.5 mm.

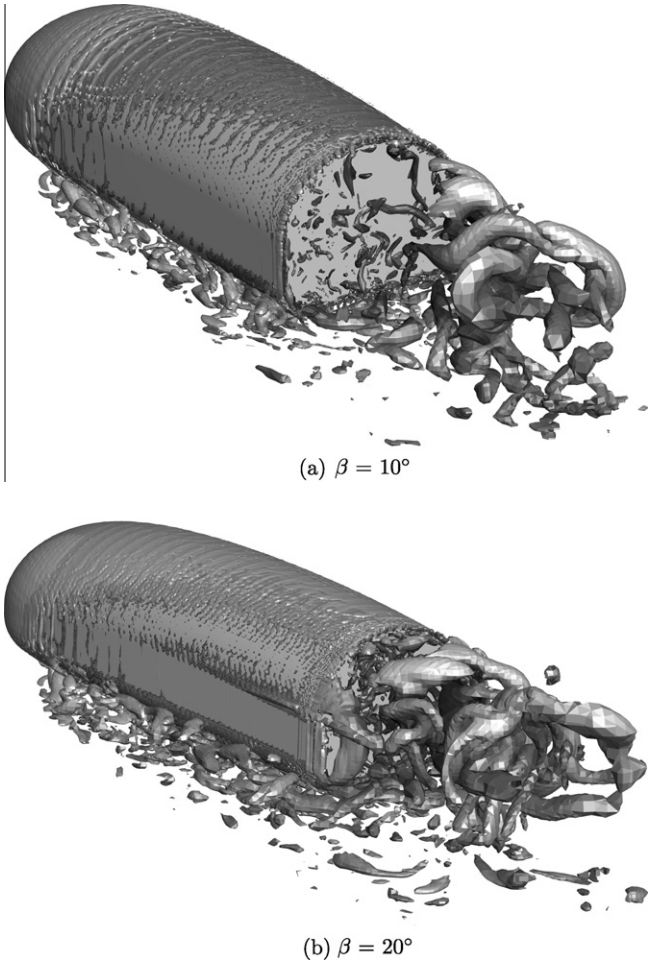

(a) $\beta = 10°$

(b) $\beta = 20°$

Fig. 8. Instantaneous flow structure – Isosurface of the second invariant $Q = 800$.

3.2. Turbulence modeling

A DES approach is based on an implicit splitting of the computational domain into two zones. In the first region near solid walls, the conventional RANS equations have to be solved. Within the second region, the governing equations are the filtered Navier–Stokes equations of the LES approach. The DES model was originally based on the Spalart–Allmaras one equation RANS turbulence model [33]. The hybrid nature of DES is not linked with any specific turbulence model [35] and the model employed in the present study is a variant based on the $k-\omega$ SST turbulence model.

The DES modification in the SST model is applied to the dissipation term in the k transport equation. Initially, the dissipation term is written as:

$$\rho\varepsilon = \beta^* \rho k \omega \tag{2}$$

where ε is the dissipation rate, β^* is a constant of the SST model, k is the turbulent kinetic energy and ω is the specific dissipation rate of turbulent frequency. For the SST–DES, this term is written now

$$\rho\varepsilon = \beta^* \rho k \omega F_{\mathrm{DES}} \tag{3}$$

with

$$F_{\mathrm{DES}} = \max\left(\frac{L_t}{C_{\mathrm{DES}}\Delta}, 1\right) \tag{4}$$

where Δ is the maximum local grid spacing ($\Delta = \max(\Delta x, \Delta y, \Delta z)$), L_t is the turbulent length scale, $L_t = \sqrt{k}/(\beta^*\omega)$ and C_{DES} is a constant. In the initial version of the SST–DES [25], C_{DES} was 0.61. In the ISIS–CFD solver, we prefer to use the value $C_{DES} = 0.78$ recommended by Menter and Kuntz [23].

4. Computational details

The computational domain starts at 3.91L in front of the model and extends to 5.39L behind the model. The width of the domain is 3L, and its height is 1.6L. The mesh is generated using HEXPRESS™, an automatic unstructured mesh generator developed by NUMECA International. This software generates meshes containing only hexahedrons. No-slip boundary condition is applied at the surface of the car model, while wall function is applied at the wind tunnel floor. This treatment for wall boundary condition, is the same as the approach adopted by Krajnović and Davidson [17], who performed LES simulations around a generic ground model. At the outlet of the computational domain, the pressure is prescribed, while for the other boundaries a Dirichlet condition for the velocity and turbulence is employed.

The time step is set to $\Delta t = 3 \times 10^{-5}$ s and 20 non-linear iterations are performed for each time step to reduce the non-linear residuals by two orders of magnitude. The flow is averaged during an non-dimensional averaging time of $t\,V_0/L = 12$. This averaging time represents 13,500 time steps.

To investigate the grid-dependency issue, computations have been performed at the yaw angle $\beta = 10°$ for three meshes with approximatively 1.6×10^6 points, 6.6×10^6 points and 10.8×10^6 points, which will be noted later on as G0, G1 and G2, respectively. Close to the wall of the model, the grid G2 has $\Delta x = 1.6$ mm in the streamwise direction, and 0.7 mm $\leqslant \Delta y \leqslant$ 1.7 mm in the direction parallel to the surface and normal to the streamwise direction. The characteristics of these meshes are detailed in Table 1. Computation with G2 requires about 5000 h of CPU time with an IBM Power 6 processor.

Fig. 2 presents the pressure coefficient along the curve (Pt) of the model versus the mesh for $\beta = 10°$. We can observe that the

Please cite this article in press as: Guilmineau E et al. Cross wind effects on a simplified car model by a DES approach. Comput Fluids (2011), doi:10.1016/j.compfluid.2011.08.020

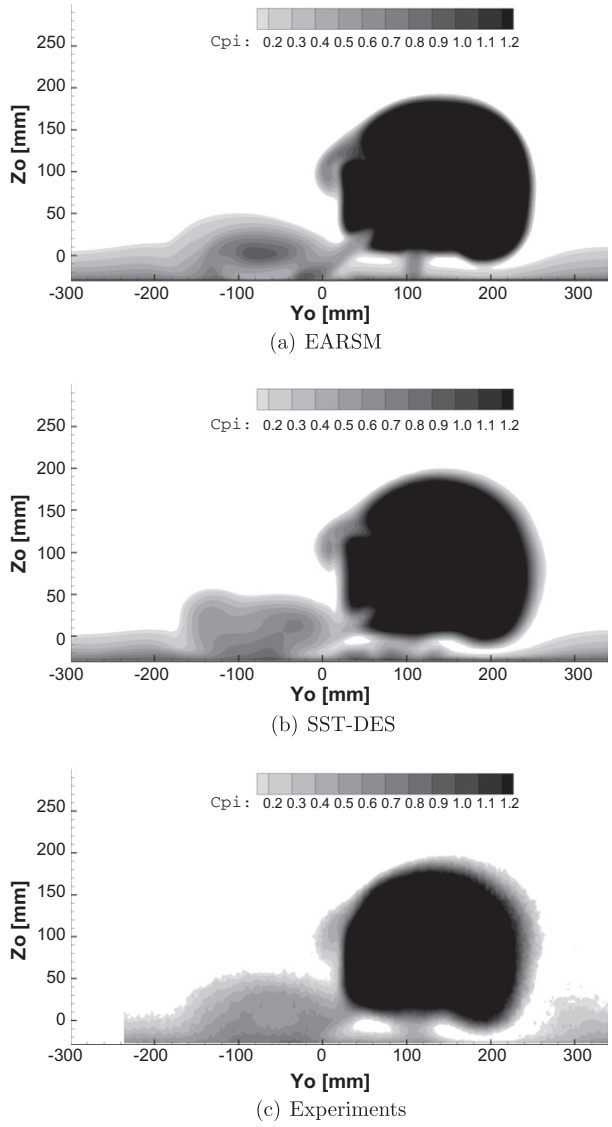

Fig. 9. Total pressure coefficient for the yaw angle $\beta = 20°$ in the Xo-plane Xo/$L = 0.60$.

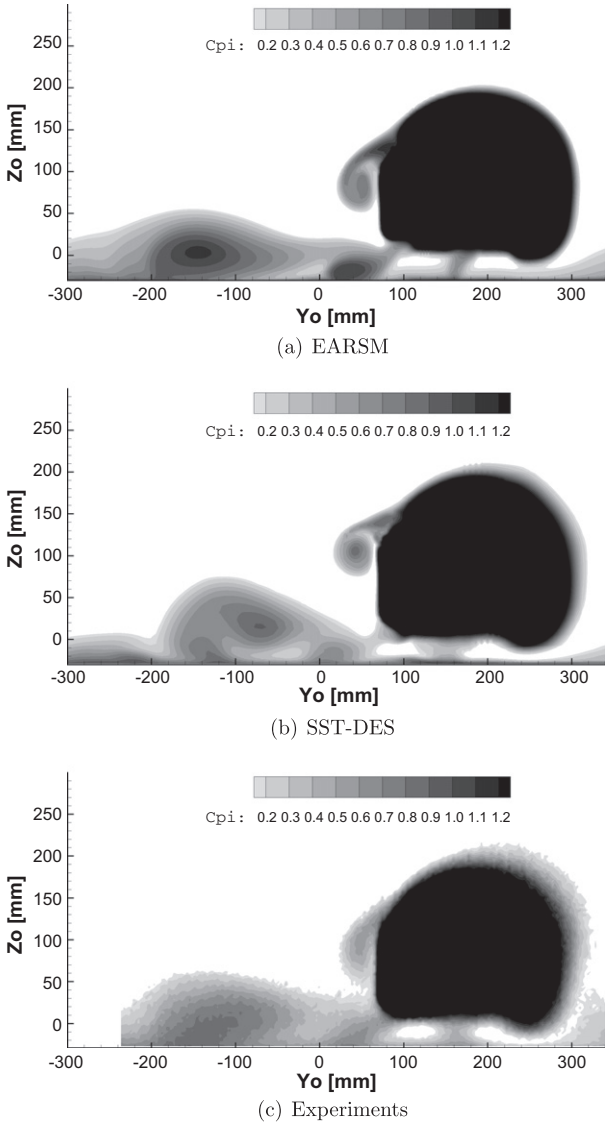

Fig. 10. Total pressure coefficient for the yaw angle $\beta = 30°$ in the Xo-plane Xo/$L = 0.55$.

predicted pressure distribution along the curve (Pt) is nearly grid independent.

Table 2 presents the drag coefficient versus the mesh. It can be observed that the difference between G1 and G2 is negligible. Those observations suggest that the grid G1 is fine enough. Hence, all the numerical results presented thereafter were obtained on grids with a density similar to grid G1, i.e. with approximatively 6.6×10^6 points.

In the near wake region, the grid size of the mesh G1 is compared with different characteristic length scales commonly employed in homogeneous isotropic turbulence study [28]. Estimations of the Kolmogorov η and Taylor λ_T length scales are proposed by Howard and Pourquie [11] for the Ahmed body wake: $\eta \approx 1.2Re^{-0.75}$ and $\lambda_T \approx 5.5\mathrm{Re}^{0.5}$. The length scale l_0 of the largest anisotropic structures containing energy may be estimated by $l_0 \sim \eta \mathrm{Re}^{3/4}$. Then the inertial range lies from $l_{EI} \sim l_0/6$, between the anisotropic large eddies and the isotropic small eddies, to $l_{DI} \sim 60\eta$, between the inertial and dissipative range. The viscous boundary sublayer at the end of the vehicle is $\eta_{nw} \approx 6.71\mathrm{Re}^{-0.9}$, which equals 1 in wall units. For the Willy model, all these length scales are given in Table 3.

The smallest grid spacings are in the vicinity of the body surface in order to resolve the surface shear stress. The wall spacing is approximatively 6×10^{-3} mm or 9×10^{-6} L. Close the base of the model, the grid spacing is 6 mm. From these values, it can be seen that the grid has its smallest meshes of the same order as the Taylor scale. Thus, according Howard and Pourquie [11], the grid is appropriate for the precision required for LES and for DES therefore.

The spatial resolutions of the first cell layer at the model obtained from the mesh G1 are shown in Table 4, where u^* is the friction velocity, n is the distance between the first node and the Willy model in the wall direction, Δs is the cell width in the streamwise direction, and Δl is the cell width in the spanwise direction.

5. Results

The numerical results obtained with the DES simulations presented in this paper will be compared to experimental data and previous numerical results that have been published recently [8]. These previous numerical results have been obtained with a nonlinear anisotropic turbulence model, the model EARSM, and a very

Please cite this article in press as: Guilmineau E et al. Cross wind effects on a simplified car model by a DES approach. Comput Fluids (2011), doi:10.1016/j.compfluid.2011.08.020

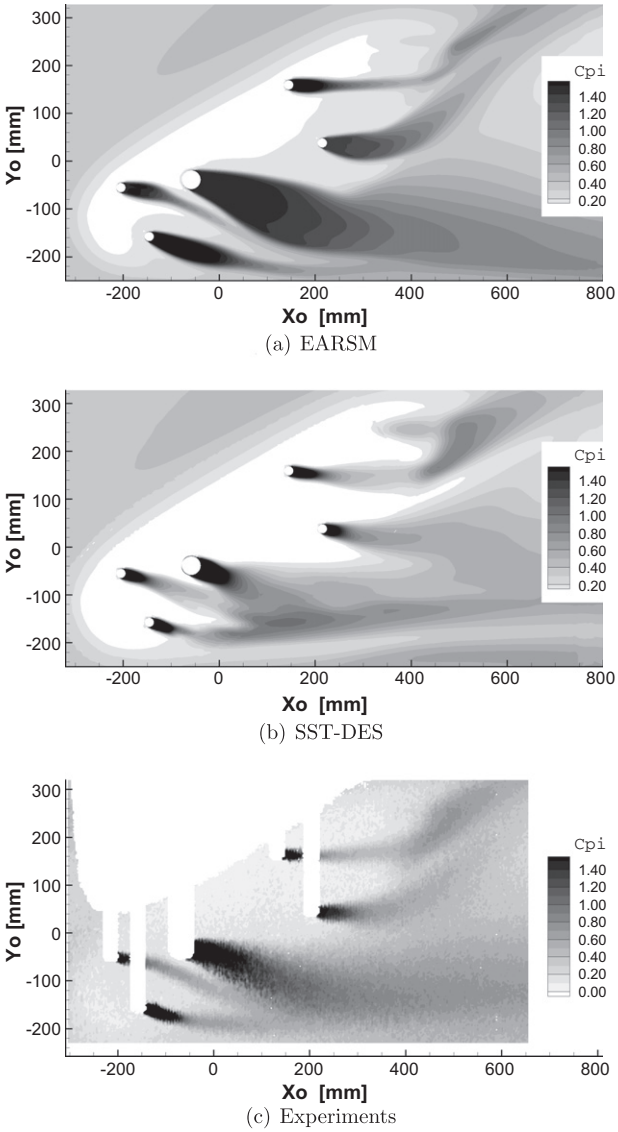

(a) EARSM

(b) SST-DES

(c) Experiments

Fig. 11. Total pressure coefficient for the yaw angle $\beta = 30°$ at Zo = −14.5 mm.

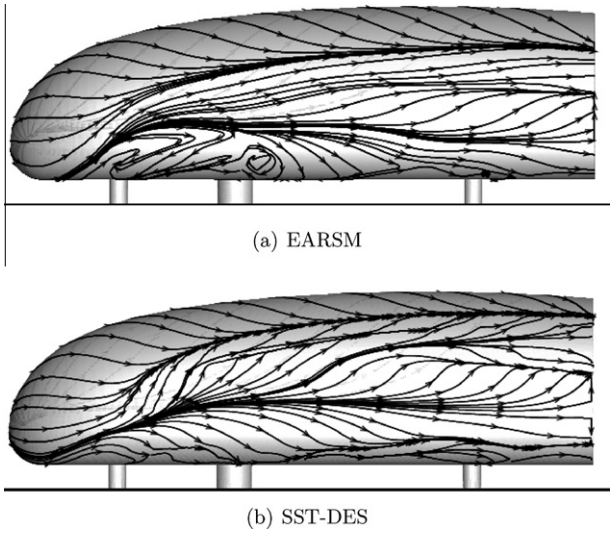

(a) EARSM

(b) SST-DES

Fig. 12. Friction lines on the leeward side at $\beta = 30°$.

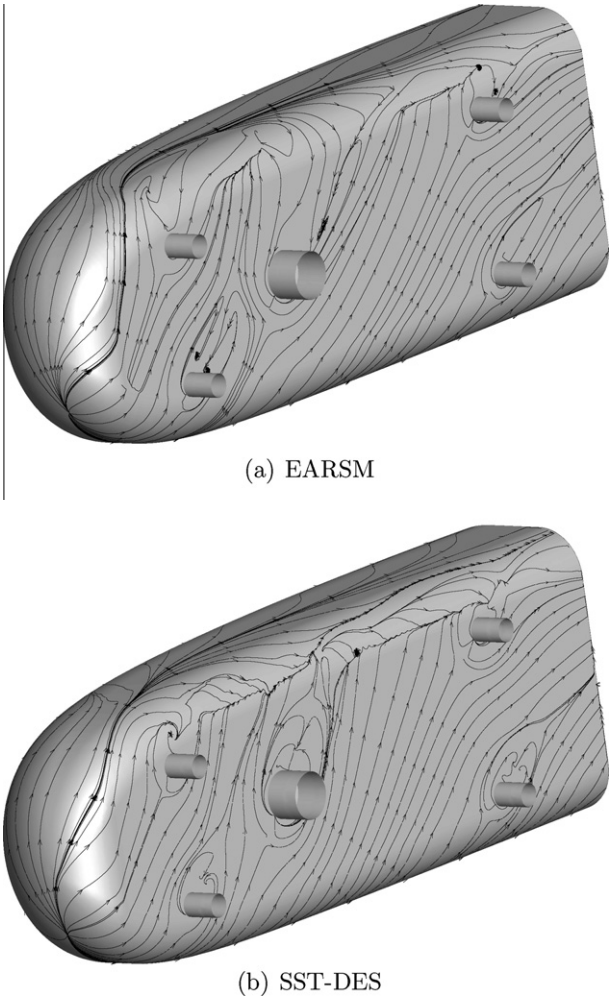

(a) EARSM

(b) SST-DES

Fig. 13. Friction lines on the underbody at $\beta = 30°$.

fine mesh composed of approximately 20 million nodes. In these previous study, the computations were steady simulations and the CPU time with an IBM Power 6 processor was approximatively 4200 h.

Unless specially specified in the paper, all results obtained by DES approach are time-averaged results.

5.1. Flow structure

Fig. 3 illustrates the wind flow over the model in the symmetry plane. The rounded nose shows a stagnation point at a height $Z = 0.1L$ (=67.6 mm), in agreement with Gohlke et al. [6] while their model does not retain the central cylinder (c). The wake displays a recirculation bubble limited by the reattachment point downstream with a length of $0.44L$ (=297 mm). In experiments [6], this length is $0.4L$ (=270 mm) while for the RANS simulation with the turbulence model EARSM [8], the recirculation length is $0.50L$ (=337 mm).

In Fig. 4, the streamlines in a Z-plane at $Z/L = 0.1588$ (=0.10719 mm), as function of the yaw angle, show the evolution of the wake of the model. At zero yaw angle, the wake is symmetric. It loses its symmetry with increased yaw angles. We can observe that the separation is limited to the end of the model and the size of the recirculation decreases as the yaw angle increases. These observations have also been noticed in the experiments [6], where the central cylinder is not present.

Please cite this article in press as: Guilmineau E et al. Cross wind effects on a simplified car model by a DES approach. Comput Fluids (2011), doi:10.1016/j.compfluid.2011.08.020

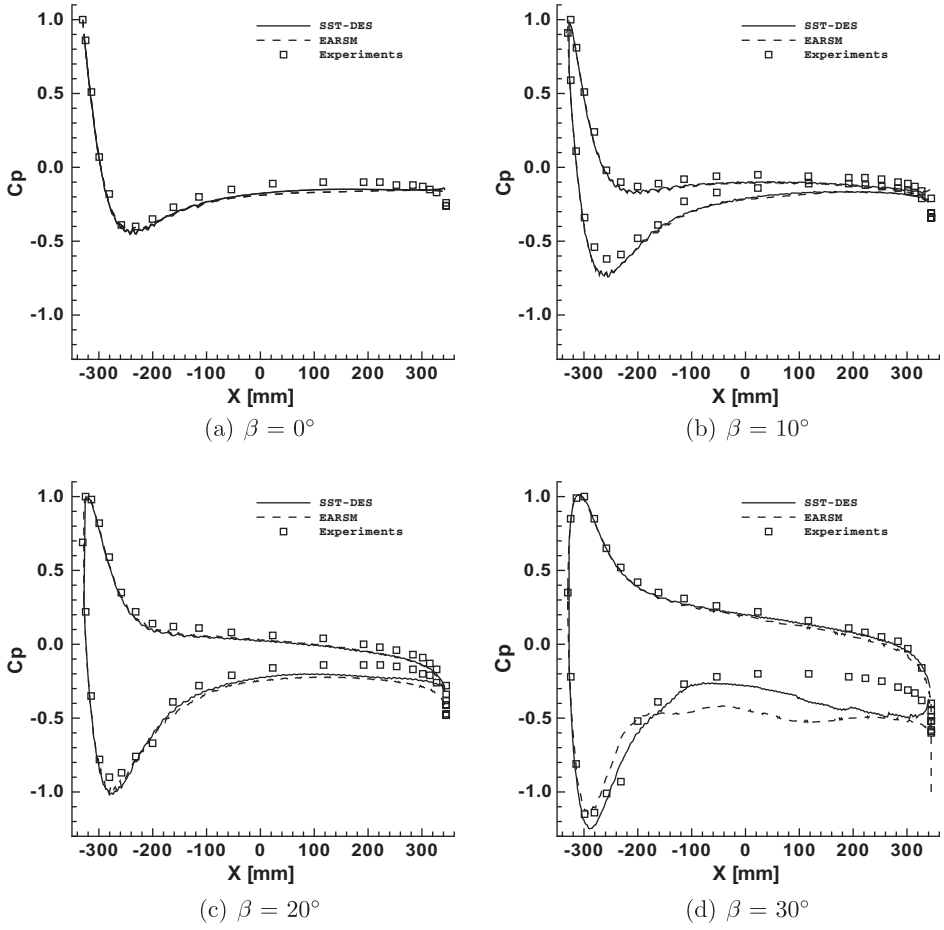

Fig. 14. Pressure coefficient along the curve (Pt).

The Fig. 5 shows the tomographies of total pressure coefficients in the Xo-plane Xo/L = 0.60 (=0.405 mm). The flow is attached to body and only a recirculation bubble appears in the wake, which confirms the previous figures. The small loss of total pressure, noted D in Fig. 5c, is due to an interaction of an upstream obstacle, not taken into account in the computation, with the boundary layer of the wind tunnel. The total pressure is lower with DES than with RANS simulation and it is in better agreement with the experimental data.

When the yaw angle increases until $\beta = 10°$, the boundary layer does not separate on the leeward side of the body, there is just a thickening of the boundary layer, as shown Fig. 6. The maximum total pressure of the left foot is higher with the RANS simulation, see Fig. 6a. This is due to the wake of the central cylinder which is larger in the RANS simulation than in DES, as shown the Fig. 7 which presents the total pressure coefficient at the middle of the ground clearance, Zo = −14.5 mm.

When the yaw angle increases, the boundary layer on the leeward side of the model continues to thicken until a separation appears. This is clearly visible in Fig. 8 that shows the instantaneous flow structure around the Willy model using the isosurface of the second invariant of velocity gradient. For the yaw angle $\beta = 10°$, no vortex appears on the leeward side of the model while at the yaw angle $\beta = 20°$, this vortex exists.

For the yaw angle $\beta = 20°$, this separation is also visible in Fig. 9. We can see also another zone, where the total pressure coefficient is high towards Yo = −100 mm. The region is due to the interaction of the left front foot and the central cylinder. We can do the same remark as the previous yaw angle, which is the maximum total pressure in the wake of the feet is larger with RANS simulation than DES.

For the yaw angle $\beta = 30°$, the position of the vortex located on the leeward side of the model and its size differ in both numerical simulations, that is visible in Fig. 10 which presents the total pressure coefficient in the plane Xo/L = 0.55 (=0.37125 mm). The vortex emanating from the central cylinder and the front feet is further away from the model. We see again that in this vortex the maximum total pressure is larger with RANS simulation than DES.

The numerical and experimental tomographies of total pressure coefficient obtained in a horizontal plane at Zo = −14.5 mm, at midpoint of the ground clearance, are drawn in Fig. 11. We observe that the wakes of the feet and the central cylinder predicted with the RANS model are too intense while those predicted by the DES approach is in better with the experiments. Nevertheless, the intensity of the wake predicted with the DES approach is still slightly lower than that obtained experimentally.

The friction lines on the leeward side, shown in Fig. 12, indicate the presence of two dominant vortical structures at the large yaw angle. We observe that the wake of the front feet and the central cylinder follows the bottom of the Willy model. This is coherent with Fig. 11 which presents the total pressure coefficient. With a DES approach, we can also observe that the vortical structure, located on the upper part of the Willy model, has a higher intensity than the RANS approach. The underbody flow patterns for the yaw angle $\beta = 30°$ is represented in Fig. 13. The wake of the cylinders is different according to the turbulence model used. With the DES approach, the wake of the front and central cylinders are weaker, and the formation of separation line starts at the left front foot and

Please cite this article in press as: Guilmineau E et al. Cross wind effects on a simplified car model by a DES approach. Comput Fluids (2011), doi:10.1016/j.compfluid.2011.08.020

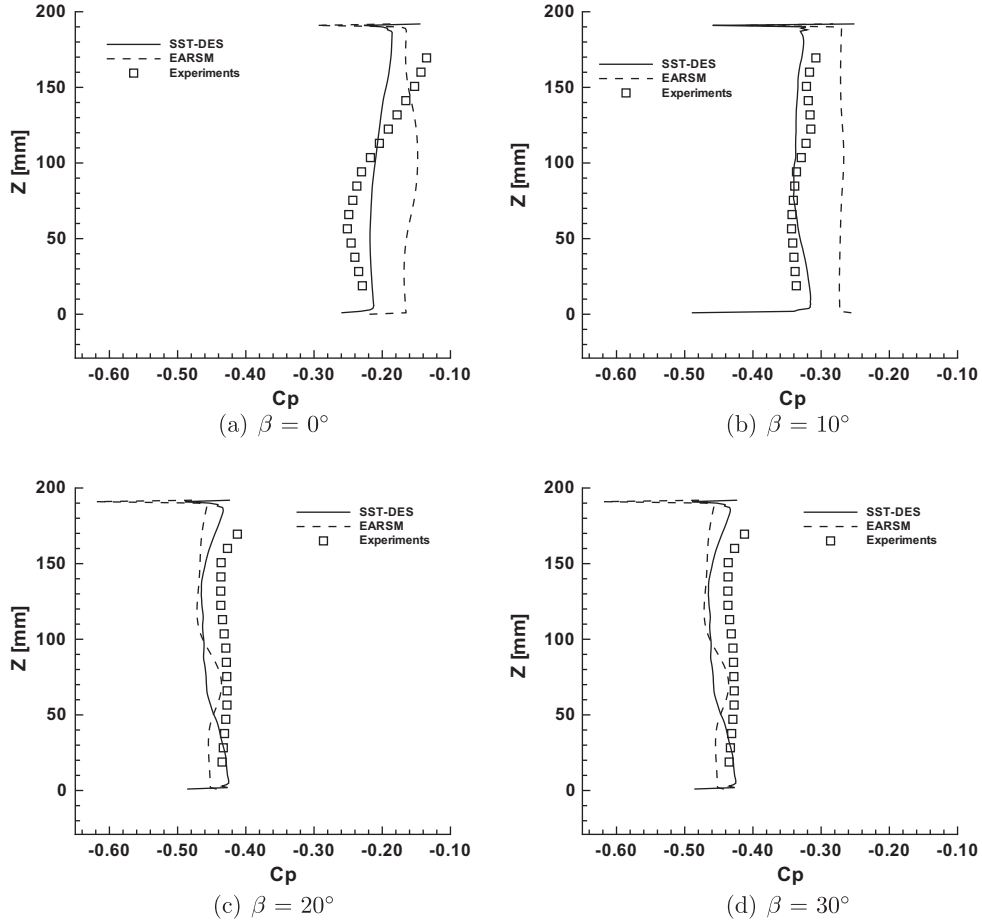

Fig. 15. Pressure coefficient on the base in the symmetry plane.

ends at the left back foot. With the RANS formulation, the wake of the central cylinder disturbs the formation of this line.

5.2. Wall pressure and forces

The evolution of the pressure coefficient Cp along curve (Pt) is drawn in Fig. 14 for different yaw angles β. The pressure predicted with the EARSM turbulence model is also presented. The results show that the pressure at the stagnation point is correctly predicted for all the yaw angles. On the windward side, wall pressure is correctly simulated by both turbulence models and for each yaw angle. For the leeward side and for the yaw angle until 10°, the numerical results are independent of the turbulence model. All turbulence models predict the same solution. For a large yaw angle, $\beta = 20°$, the differences start to become visible. For the yaw angle $\beta = 30°$, the differences between the numerical simulations are apparent. The pressure increases when we move to the front from the end of the model until $X = -200$ mm for the RANS simulation and until $X = -100$ mm for the DES. In experiments, the pressure increases until $X = -50$ mm. Results obtained by LES [18] show that the LES predicition is better but only at the end of leeward side.

The pressure coefficient in the symmetry plane on the base of the model is presented in Fig. 15 for several yaw angles. For the yaw angles up to 10°, the results obtained with the RANS simulations over-predict the pressure coefficient while for the other yaw angles, the level of pressure is in better agreement while the shape presents a bump in the low region of the base. Moreover, the position of the maximum pressure, obtained with the RANS simulations, goes down when the yaw angle increases. With DES, the agreement is improved, except at the yaw angle $\beta = 0°$, where, close to the top of the model, the pressure is under-estimated.

Fig. 16 shows the pressure distribution on the base of the model at $Z = 50$ mm. Again, the pressure is over-estimated with the RANS simulations for the yaw angles up to 10°. Moreover, the pressure is almost uniform. The pressure does not change toward a maximum near the windward side, contrary to DES simulations which exhibit a spatial evolution similar to the experimental measurements. For the yaw angle 30°, the maximum pressure obtained with the EARSM turbulence model is located close to the symmetry plane while, close to the windward side, the pressure is uniform. Furthermore, the base pressure level seems to be fairly well predicted when the DES approach is used.

The drag, see Fig. 17, increases up to the yaw angle $\beta = 20°$. After this angle, the drag decreases as the yaw angle increases. This behavior is typical of a square-back model [12]. For the small yaw angles and up to $\beta = 20°$, the numerical prediction with the EARSM turbulence model under-evaluates the drag. This result is in agreement with the fact that for these yaw angles, the pressure on the base is over-predicted. In fact, for bluff bodies, the drag is mainly due to the pressure and as the pressure on the base is over-estimated, this leads to an underestimation of the drag force. The drag predicted with the DES simulation is in better agreement with the experimental measurements, and for all yaw angles, the drag is overestimated. The side force, see Fig. 18, shows a linear evolution. Again, the agreement with the experimental data is better with DES than with the RANS simulations. If we compare with LES prediction [18], the drag coefficient obtained by the DES approach is very similar, but for the side force coefficient, the DES formulation

Please cite this article in press as: Guilmineau E et al. Cross wind effects on a simplified car model by a DES approach. Comput Fluids (2011), doi:10.1016/j.compfluid.2011.08.020

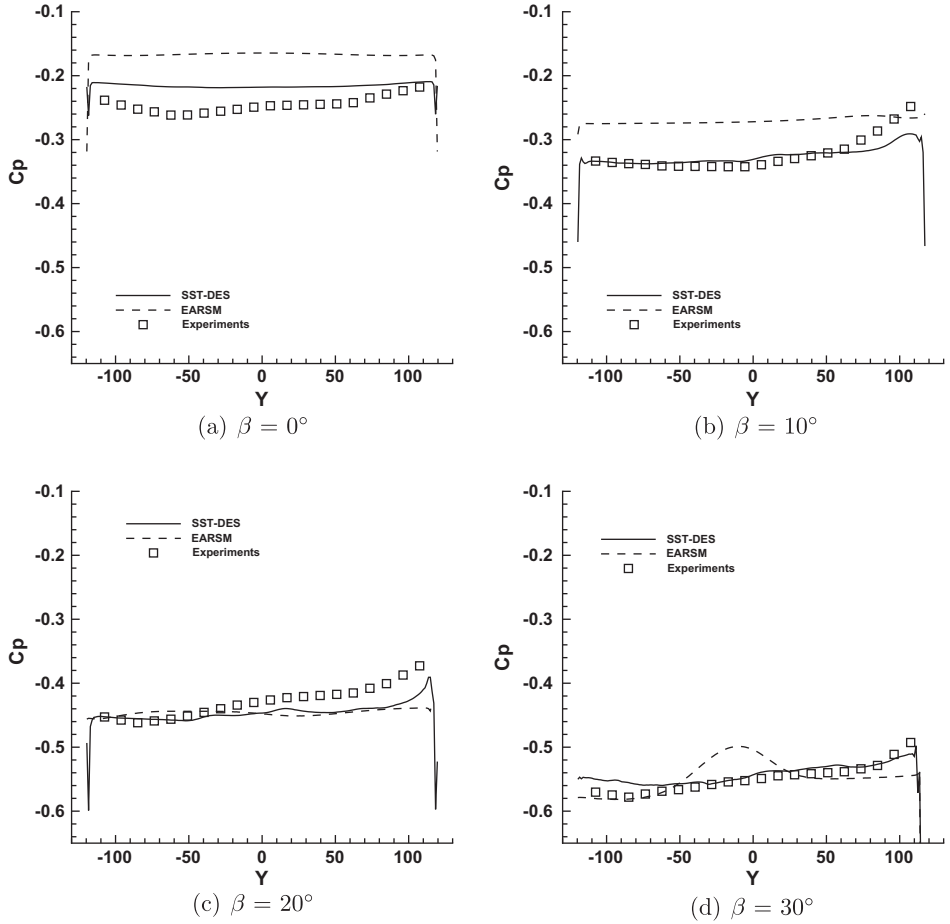

Fig. 16. Pressure coefficient on the base at $Z = 50$ mm.

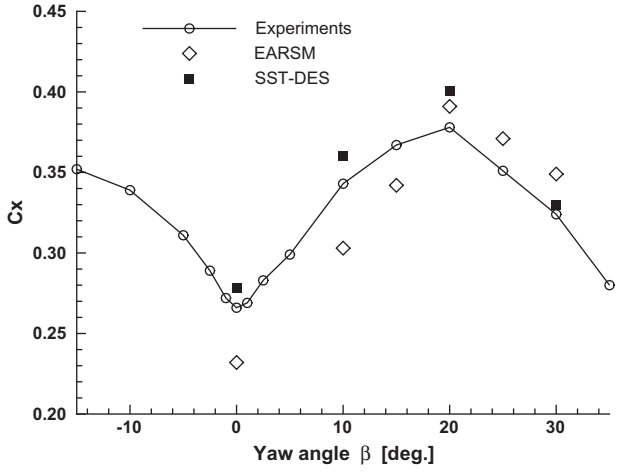

Fig. 17. Drag coefficient Cx versus the yaw angle β.

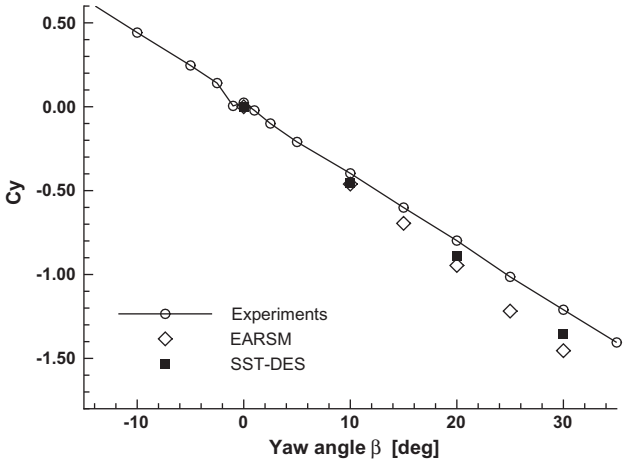

Fig. 18. Side force coefficient Cy versus the yaw angle β.

gives a better prediction than LES [18]. The yawing moment versus the yaw angle is presented in Fig. 19. This coefficient rises linearly with the yaw angle up to $\beta = 25°$. The linearity of the side force and the yawing moment are typical characteristics of real vehicles [12]. The result obtained at the yaw angle $\beta = 30°$ with the EARSM turbulence model shows a decrease of the yawing moment while with DES, the yawing moment continues to increase with a reduced increasing rate, in agreement with the experimental measurements. It would be interesting to compare this result with the LES simulation given by [18]. Unfortunately, result for this quantity is unavailable in [18].

To analyze the contribution of different regions to the forces and moments, the model is divided into a front and a rear part at $X/L = 0$. Each of these two parts is divided into an upper and a lower zone at $Z/L = 0.11$ and into a leeward and windward region at $Y/L = 0$. As in bluff-body aerodynamics, the friction term is neglected, only the pressure contribution is examined.

Please cite this article in press as: Guilmineau E et al. Cross wind effects on a simplified car model by a DES approach. Comput Fluids (2011), doi:10.1016/j.compfluid.2011.08.020

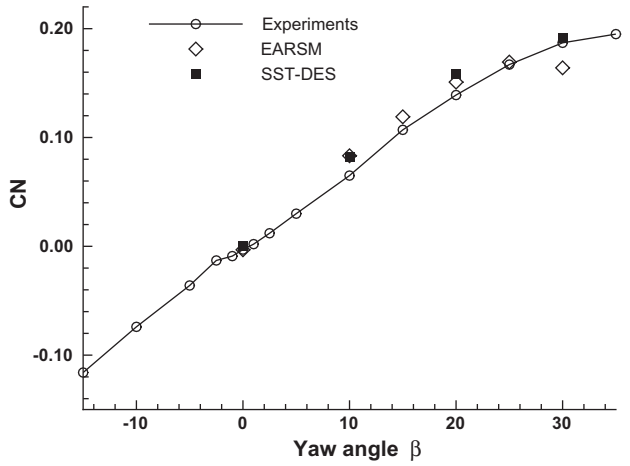

Fig. 19. Yawing moment coefficient versus the yaw angle β.

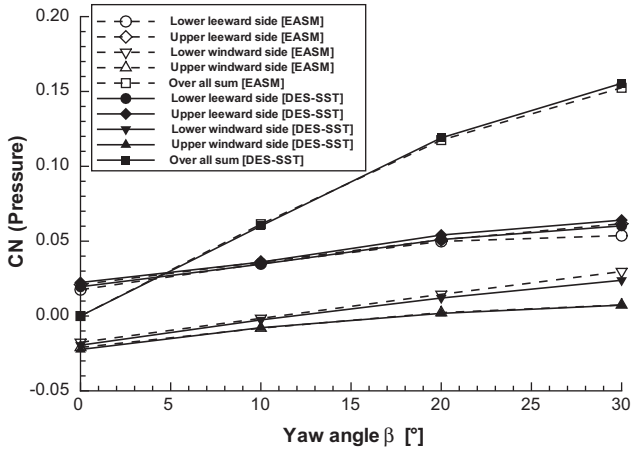

(a) Front part

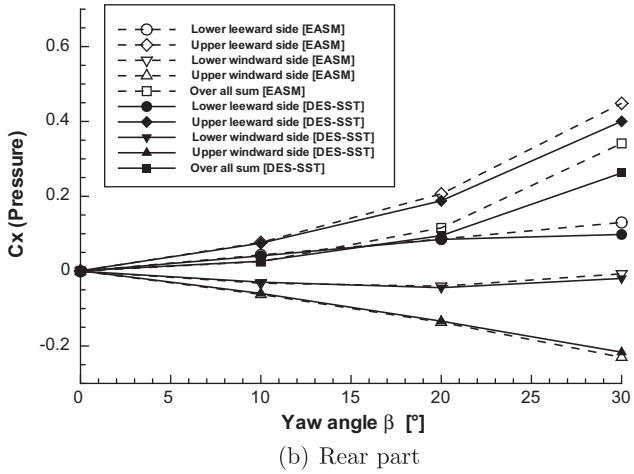

(b) Rear part

Fig. 20. Pressure yawing moment coefficient versus the yaw angle β.

Fig. 20a shows the contribution per zone to the pressure yawing moment of the front of the model. We can observe that each part has a positive slope. The leeward side has a larger contribution to the yawing moment than the windward side. The pressure yawing moment rises linearly up to the yaw angle $\beta = 20°$. After this yaw angle, the slope of the curve changes but always with a positive gradient. There is more difference between the upper and lower sides for the windward side than for the leeward side. Between both simulations, the differences are much more important for the lower side than for the upper side. Moreover, this difference increases with the yaw angle and the difference is more important for the leeward side than for the windward side. This is linked with the friction lines on the model, see Figs. 12 and 13 which present the friction lines on the leeward side and the underbody, respectively. With the RANS simulation, the wakes of all feet are very stretched and the flow on the lower part of the model is different. For both simulations, these zones create a positive contribution of the yawing moment.

The pressure yawing moment of the rear half, see Fig. 20b, decreases as the yaw angle increases and the rear part has a counter-rotating contribution to the global yawing moment. The largest contribution to the pressure yawing moment comes from the upper leeward side. The largest difference between both simulations appear on the leeward side of the model. However, both simulations have the same tendency. The friction lines on the rear part, shown in Fig. 12, indicate the presence of two dominant vortical structures on the leeward side at the large yaw angle.

6. Conclusions

The objective of this paper is to simulate the flow around a generic passenger vehicle in cross wind conditions, with respect to experimental data. The test case is a square-back model, which has been specifically designed for the analysis of side wind effects on automobiles. Simulations are performed using Detached Eddy Simulations, and the averaged flow on the model is investigated at several yaw angles from 0° to 30°.

All numerical results are compared with experimental data and previous numerical data obtained with a previous EARSM RANS simulation. This RANS simulation was obtained with a very fine mesh composed of approximatively 20 million nodes and 4200 h of CPU time were necessary. In this paper, the DES computations were performed on a mesh coarser than that used for RANS simulations and 5000 h of CPU were needed which is more than the CPU used for the RANS simulation with a fine mesh.

With the DES approach, the numerical forces and moment coefficients, the wall pressure, and the total pressure in the wake are much better predicted compared with RANS approach. The pressure evolution on the car model, especially on the base of the model except for the yaw angle $\beta = 0°$, has been recovered. These results confirm the capability of the DES approach implemented in the ISIS–CFD flow solver to capture the physics of three-dimensional separated flows around a square-back model for which the leeward separations take place on smooth surfaces and are not imposed by sharp corners except the base. The typical characteristics of the model, such as drag, side force, and yawing moment coefficients, are correctly reproduced. At large yaw angles, a DES formulation provides a far better prediction than a RANS simulation.

However, a mismatch of the pressure close to the base on the leeward side between the experimental data and the numerical results obtained by the DES approach suggests that modelizing error and/or discretization error still exists. Nevertheless, the present results are encouraging, suggesting that the DES formulation can be used to model in the future the flow around a car with rotating wheels and a moving ground.

Acknowledgments

This work was granted access to the HPC resources of CINES and IDRIS under the allocation 2009-[20129] made by Grand

Equipement National de Calcul Intensif (GENCI) which is gratefully acknowledged.

References

[1] Ahmed SR, Ramm G, Faltin G. Some salient features of the time-averaged ground vehicle wake. SAE paper 840300; 1984.
[2] Bayraktar I, Landman D, Baysal O. Experimental and computation investigation of Ahmed body for ground vehicle aerodynamics. SAE paper 2001-01-2742; 2001.
[3] Charuvisit S, Kimura K, Fujino Y. Experimental and semi-analytical studies on the aerodynamic forces acting on a vehicle passing through the wake of a bridge tower in cross wind. J Wind Eng Ind Aerodynam 2004;92:749–80.
[4] Chometon F, Strzelecki A, Laurent J, Assaoui E. Experimental analysis of unsteady wakes on a new simple car model. In: Fifth international colloquium on bluff body aerodynamics and applications. Ottawa (Ontario, Canada); 2004. p. 545–8.
[5] Fares E. Unsteady flow simulation of the Ahmed reference body using a Lattice Boltzmann approach. Comput Fluids 2006;35:940–50.
[6] Gohlke M, Beaudoin JF, Amielh M, Anselmet F. Experimental analysis of flow structures and forces on a 3D-bluff-body in constant cross-wind. Exp Fluids 2007;43(4):579–94.
[7] Gohlke M, Beaudoin JF, Amielh M, Anselmet F. Thorough analysis of vortical structures in the flow around a yawed bluff body. J Turbul 2008;9(15):1–28.
[8] Guilmineau E, Chometon F. Effect of side wind on a simplified car model: experimental and numerical analysis. J Fluids Eng 2009;31(2).
[9] Han T. Computational analysis of three-dimensional turbulent flow around a bluff body in ground proximity. AIAA J 1989;27(9):1213–9.
[10] Hemida HN. Large-eddy simulation of the flow around simplified high-speed trains under side wind conditions. Ph.D. Thesis, Chalmers University of Technology; 2006.
[11] Howard RJA, Pourquie M. Large eddy simulation on the Ahmed reference model. J Turbul 2001;3(1).
[12] Hucho WH. Aerodynamics of road vehicles. SAE International; 1998.
[13] Issa R. Solution of the implicitly discretized fluid flow equations by operator-splitting. J Comput Phys 1985;62:40–65.
[14] Jasak H, Weller H, Gosman A. High resolution NVD differencing scheme for arbitrarily unstructured meshes. Int J Numer Methods Fluids 1999;31:431–49.
[15] Kapadia S, Roy S, Wurtzler K. Detached eddy simulation over a reference Ahmed car model. In: 41st Aerospace sciences meeting and exhibit. AIAA paper 2003-0857. Reno (NE); January 2003.
[16] Khier W, Breuer M, Durst F. Flow structure around trains under side wind conditions: a numerical study. Comput Fluids 2000;29:179–95.
[17] Krajnović S, Davidson L. Flow around a simplified car – Part 1: Large eddy simulation. J Fluids Eng 2005;127:907–18.
[18] Krajnović S, Sarmast S. Numerical investigation of the influence of side winds on a simplified car at various yaw angles. In: 3rd Joint US-European fluids engineering summer meeting. FEDSM-ICNMM2010-30766. Montreal (Canada); 2010.
[19] Leonard BP. Simple high-accuracy resolution program for convective modelling of discontinuities. Int J Numer Methods Fluids 1988;8:1291–318.
[20] Lienhart H, Becker S. Flow and turbulence in the wake of a simplified car model. SAE Paper 2003-01-0656; 2003.
[21] Maddox SM, Squires KD, Wurtzler KE, Forsythe JR. Detached-eddy simulation of the flow around the ground transportation system. In: McCallen R, Browand F, Ross J, editors. Lectures notes in applied and computational mechanics – the aerodynamics of heavy vehicles: trucks, buses and trains, vol. 19. Springer-Verlag; 2004. p. 89–104.
[22] McCallen R, Flowers D, Dunn T, Owens J, Browand F, Hammache M, et al. Aerodynamic drag of heavy vehicles (class 7–8): Simulation and benchmarking. SAE Paper 2000-01-2209; 2000.
[23] Menter FR, Kuntz M. A zonal SST–DES formulation. DES Workshop, St Petersburg; 2003.
[24] Menter FR, Kuntz M. Adaptation of eddy-viscosity turbulence models to unsteady separated flow behind vehicles. In: McCallen R, Browand F, Ross J, editors. Lectures notes in applied and computational mechanics – the aerodynamics of heavy vehicles: trucks, buses and trains, vol. 19. Springer-Verlag; 2004. p. 339–52.
[25] Menter FR, Kuntz M, Langtry R. Ten years of industrial experience with the SST turbulence model. In: Hanjalić K, Nagano Y, Tummers M, editors. Turbulence, Heat and Mass Transfer 4, vol. 19. Begell House, Inc.; 2003. p. 339–52.
[26] Minguez M, Pasquetti R, Serre E. High-order large eddy simulation of flow over the "Ahmed body" car model. Phys Fluids 2008;20.
[27] Ortega J, Salari K, Storms B. Investigation of tractor base bleeding for heavy vehicle aerodynamic drag reduction. In: McCallen R, Browand F, Ross J, editors. Lectures notes in applied and computational mechanics – the aerodynamics of heavy vehicles II: Trucks, buses and trains, vol. 41. Berlin/Heideberg: Springer; 2009. p. 161–78.
[28] Pope SB. Turbulence flows. Cambridge University Press; 2000.
[29] Queutey P, Visonneau M. An interface capturing method for free-surface hydrodynamic flows. Comput Fluids 2007;36:1481–510.
[30] Rhie C, Chow W. A numerical study of the turbulent flow past an isolated aerofoil with trailing edge separation. AIAA J 1983;17:1525–32.
[31] Sims-Williams DB, Duncan BD. The Ahmed model unsteady wake: experimental and computational analyses. SAE Paper 2003-01-1315; 2003.
[32] Spalart PR, Allmaras S. A one-equation turbulence model for aerodynamic flows. In: AIAA 30th aerospace sciences meeting. AIAA Paper 92-0439. Reno (NV); 1992.
[33] Spalart PR, Jou W, Strelets M, Allmaras S. Comments on the feasibility of LES for wings and on a hybrid RANS/LES approach. In: Liu CZ, editor. 1st AFOSR international conference on DNS/LES. Advances in DNS/LES. Greyden Press; 1997.
[34] Spohn A, Gilliron G. Flow separations generated by a simplified geometry of an automotive vehicle. In: IUTAM symposium on unsteady separated flows. Toulouse, France; April 2002.
[35] Strelets M. Detached eddy simulation of massively separated flows. AIAA paper 2001-0879; 2001.
[36] Tsubokura M, Kobayashi T, Nakashima T, Nouzawa T, Nakamura T, Zhang H, et al. Computational visualization of unsteady flow around vehicles using high performance computing. Comput Fluids 2009;38:981–90.
[37] Tsubokura M, Takahashi K, Matsuuki T, Nakashima T, Ikenaga T, Kitoh K, 2010. HPC–LES for unsteady aerodynamics of a heavy duty truck in wind gust – 1st report: validation and unsteady flow strucures. SAE paper 2010-01-1010.

Please cite this article in press as: Guilmineau E et al. Cross wind effects on a simplified car model by a DES approach. Comput Fluids (2011), doi:10.1016/j.compfluid.2011.08.020